Available online at www.sciencedirect.com
SCIENCE DIRECT
Journal of Power Sources 154 (2006) 268–272
JOURNAL OF POWER SOURCES
www.elsevier.com/locate/jpowsour

Short communication

# Enhancement of the electrochemical properties of *o*-$LiMnO_2$ cathodes at elevated temperature by lithium and fluorine additions

Tae-Joon Kim [a], Dongyeon Son [a], Jaephil Cho [b], Byungwoo Park [a,*]

[a] *School of Materials Science and Engineering, Research Center for Energy Conversion and Storage, Seoul National University, Seoul, Korea*
[b] *Department of Applied Chemistry, Kumoh National Institute of Technology, Gumi, Korea*

Received 14 January 2005; accepted 11 March 2005
Available online 9 June 2005

**Abstract**

Orthorhombic $LiMnO_2$ cathodes suffer severe capacity fading due to accelerated manganese dissolution at elevated temperatures. Fluorine-modified $LiMnO_2$ cathodes prepared by a solid-state reaction show less cation mixing and a well-defined crystallinity with a larger grain/powder morphology. The cathodes exhibit improved capacity retention and rate capability at the elevated temperature (55 °C) compared with undoped counterparts.


*Keywords:* *o*-$LiMnO_2$ cathode; Li and F additions; Elevated-temperature cycling; Lithium-ion batteries; Capacity fading; Rate capability

## 1. Introduction

Lithium-manganese-oxide is a candidate material to replace the commercial $LiCoO_2$ cathode in lithium-ion secondary batteries, because it has the advantages of lower toxicity and cost [1–5]. Unfortunately, however, one of the choices, $LiMn_2O_4$, delivers a lower discharge capacity (110–120 mAh $g^{-1}$) than $LiCoO_2$ (140–150 mAh $g^{-1}$) [1–5]. Moreover, it faces severe capacity fading problems due to accelerated dissolution of manganese on cycling at elevated temperature (>50 °C), and structural instability due to Jahn–Teller (J–T) distortion [5–9]. Orthorhombic $LiMnO_2$ (*o*-$LiMnO_2$) has a high theoretical capacity (∼285 mAh $g^{-1}$) and a better cycleability than $LiMn_2O_4$ over a wide voltage range [10,11], but its cycling performance is poor at the elevated temperature [11].

It has been reported that *o*-$LiMnO_2$ transforms to a phase with a spinel-like structure during cycling [12]. The dissolution of manganese is again the cause of poor cycling performance at the elevated temperature and leads to defective spinels [13]. The dissolution is induced by acids generated from reaction of $LiPF_6$ salts with the water impurities present in the cell [14,15]. Robertson et al. [16] suggested that the capacity decay is due to disproportionation of the spinel electrode into acid-soluble species.

Croguennec et al. [17] reported that small crystallites of 1–10 μm are more easily transformed into a spinel-like structure. They showed that *o*-$LiMnO_2$ has stacking faults (local regions of monoclinic ordering) that are caused by structural disorder between the Li and Mn sites, and that these stacking faults induce a broadening of the (1 1 0) diffraction peak [17,18]. Orthorhombic $LiMnO_2$ cathodes with more stacking faults underwent an easier phase transformation from an orthorhombic to a spinel structure with more severe capacity fading on cycling, compared with samples with less stacking faults [19].

To stabilize the structural instability for elevated-temperature performance, cation substitution such as *o*-$LiAl_{1-x}Mn_xO_2$ has been studied. While capacity retention was found to be better than that of *o*-$LiMnO_2$ on cycling tests at 55 °C, Al substitution (*o*-$LiAl_{1-x}Mn_xO_2$) did not prevent J–T distortion [20]. An alternative approach to improving the structural stability is by coating the *o*-$LiMnO_2$ surface with

* Corresponding author. Tel.: +82 2 880 8319; fax: +82 2 883 8197.
*E-mail address:* byungwoo@snu.ac.kr (B. Park).

0378-7753/$ – see front matter © 2005 Elsevier B.V. All rights reserved.
doi:10.1016/j.jpowsour.2005.03.193

metal oxides, which might minimize the structural instability from HF attack [8,9].

Recently, improvements on cycleability through the co-doping of cations (Li, Mg, Al, etc.) and anions (F, S, etc.) into $LiMn_2O_4$- or $LiNiO_2$-based cathodes have been reported [21–27]. A sintering agent during synthesis can cause large and smooth powders [28,29]. Dahn's group [30] obtained dense $LiNi_xCo_{1-2x}Mn_xO_2$ materials at 900 °C by adding LiF as a sintering agent. This study reports enhancement of the electrochemical properties of *o*-$LiMnO_2$ cathodes by Li and F additions through a solid-state reaction.

## 2. Experimental

$Li_{1+x}Mn_{1-x}O_{2-y}F_y$ $(0 \le x \le 0.07,\ 0 \le y \le 0.3)$ samples were prepared by a solid-state reaction with $LiOH{\cdot}H_2O$, $Mn_2O_3$ and LiF. Heat treatment was performed at 800 °C for 20 h in an argon atmosphere. An excess amount of lithium was used to compensate for the amount lost during heat treatment. The lithium composition was analyzed by inductively coupled plasma atomic emission spectrometry (ICP–AES).

X-ray diffraction (XRD) with Cu Kα radiation (M18XHF-SRA, MAC Science) was used to determine the phases and the degree of crystallinity (stacking faults) in the 2$\theta$ range of 10–70°. Raman spectra were obtained to determine the bonding nature using LabRamHR (Jobin Yvon Co.) with Ar-ion laser excitation (514 nm). The particle size and morphology of the synthesized powders were analyzed by field-emission scanning electron microscopy (FE-SEM) with a JSM-6330F (JEOL).

Electrochemical cycling tests were performed with coin-type half cells (2016) at both elevated temperature (55 °C) and room temperature. $Li_{1+x}Mn_{1-x}O_{2-y}F_y$ active materials with a finite size were prepared for the cycling tests using a 25 μm-sized sieve. Cathodes were made from the active material, super P carbon black, and a polyvinylidene fluoride (PVdF) binder in a weight ratio of 90:5:5. The electrolyte was 1 M $LiPF_6$ with 1:1 ethylene carbonate/ethyl-methyl carbonate (EC/EMC), and lithium metal was used as the anode. The cycle-life of the cells was tested at a rate of 0.2 C (=36 mA $g^{-1}$; 1 C = 180 mA $g^{-1}$) between 4.5 and 2 V.

For XRD measurements of the cycled electrodes, the discharged cells after cycling were kept at a 2 V discharge state until the current decreased to 10% of the initial value so that the cells would be stabilized near 2 V. The cells were disassembled in a glove box ($H_2O$ level <50 ppm), and the $Li_{1+x}Mn_{1-x}O_{2-y}F_y$ powders were rinsed thoroughly with a DEC solution to remove the $LiPF_6$ salts.

## 3. Results and discussion

The XRD patterns for various lithium-manganese-oxide samples with anion-dopant fluorine before cycling are presented in Fig. 1. All the samples have a predominantly orthorhombic structure (with a space group of *Pmnm*) based on the *o*-$LiMnO_2$ structure with small amounts of *m*-$Li_2MnO_3$ phase [1]. The formation of the $Li_2MnO_3$ phase is due to reaction with oxygen in the atmosphere. Anion substitution does not cause any particular change in the lattice constants (*a*, *b* and *c*) of *o*-$Li_{1+x}Mn_{1-x}O_{2-y}F_y$. The unit-cell parameter of the undoped *o*-$LiMnO_2$ sample is $a = (4.587 \pm 0.009)$ Å, $b = (5.737 \pm 0.017)$ Å and $c = (2.801 \pm 0.008)$ Å, while that of *o*-$Li_{1.07}Mn_{0.93}O_{1.92}F_{0.08}$ is $a = (4.577 \pm 0.007)$ Å, $b = (5.751 \pm 0.013)$ Å and $c = (2.807 \pm 0.006)$ Å.

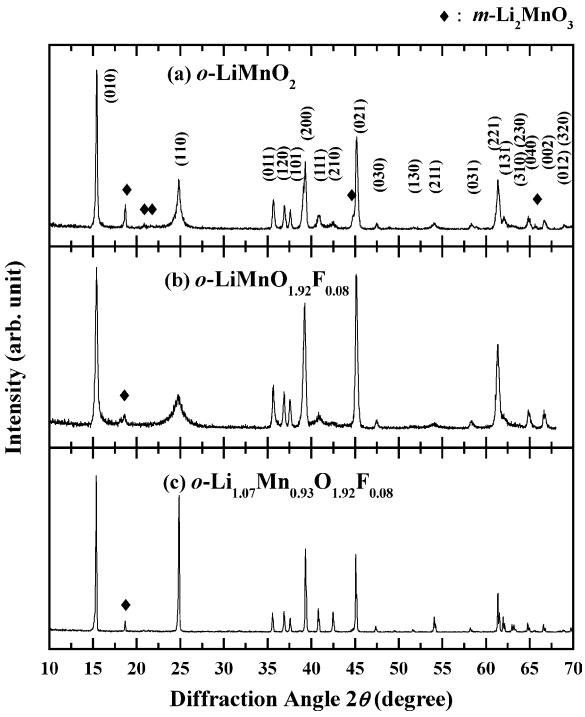


Fig. 1. X-ray diffraction patterns for various *o*-$Li_{1+x}Mn_{1-x}O_{2-y}F_y$ powders with anion-dopant F: (a) stoichiometric *o*-$LiMnO_2$; (b) *o*-$LiMnO_{1.92}F_{0.08}$; (c) *o*-$Li_{1.07}Mn_{0.93}O_{1.92}F_{0.08}$. Some *m*-$Li_2MnO_3$ phase coexists.

Monoclinic $LiMnO_2$ exists by stacking faults in *o*-$LiMnO_2$ due to cation mixing between Li and Mn, and this may influence the phase transition of *o*-$LiMnO_2$ to the spinel structure during cycling. Disorder-sensitive (1 1 0) broadening shows these stacking faults [10,17,18]. A full-width-at-half-maximum (FWHM, $\Delta(2\theta)$) of the (1 1 0) peak from each sample is approximately (a) 0.50°, (b) 1.30° and (c) 0.11°, respectively. From these results, *o*-$Li_{1.07}Mn_{0.93}O_{1.92}F_{0.08}$ has a well-developed crystalline phase, with less stacking faults than an undoped one. In similar work [21], a small quantity of fluorine was found to reduce cation mixing. The overall FWHM information of the XRD patterns (from (0 1 0), (0 1 1), (2 0 0), etc.) shows that *o*-$Li_{1.07}Mn_{0.93}O_{1.92}F_{0.08}$ has a mature crystallinity and/or a larger grain size than undoped *o*-$LiMnO_2$. The composition ratios of Li/Mn in *o*-$LiMnO_2$, *o*-$LiMnO_{1.92}F_{0.08}$ and *o*-$Li_{1.07}Mn_{0.93}O_{1.92}F_{0.08}$ were measured as 1.11, 1.11 and 1.22, respectively (instead of 1.0, 1.0 and 1.15, respectively),

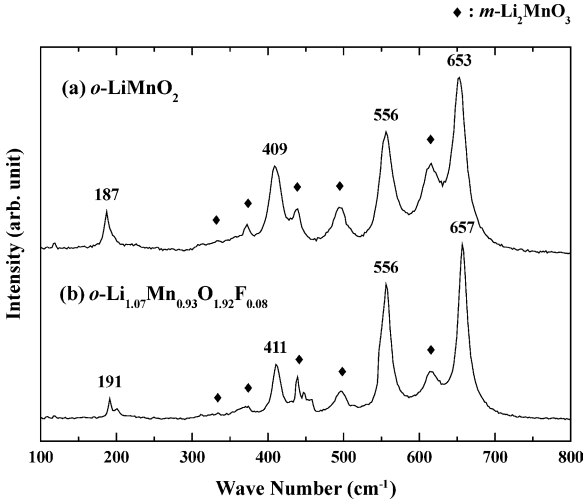


Fig. 2. Raman spectra for undoped and F-substituted $o$-$Li_{1+x}Mn_{1-x}O_{2-y}F_y$ powders.

which is probably due to the $m$-$Li_2MnO_3$ phase and grain-boundary segregation.

The overall Raman spectra of $o$-$LiMnO_2$ and $o$-$Li_{1.07}Mn_{0.93}O_{1.92}F_{0.08}$ are similar, and the change in bond energy by fluorination is negligible (Fig. 2). There is, however, a noticeable decrease in the peak width with fluorination, i.e., the peak widths (FWHMs) of the bands at ~410, ~560 and ~660 $cm^{-1}$ decrease from ~19, ~24 and ~21 $cm^{-1}$ in $o$-$LiMnO_2$ to ~15, ~17 and ~16 $cm^{-1}$ in $o$-$Li_{1.07}Mn_{0.93}O_{1.92}F_{0.08}$, respectively. The bands at ~560 and ~660 $cm^{-1}$ are attributed to the O–Mn–O bending and stretching modes, respectively [31,32]. The broadening of the Raman bands can be attributed to the occurrence of stacking faults due to cationic disorder and/or immature crystallinity of the structure. The sharper shape of the peaks in the fluorinated samples signifies better crystallinity and less cation mixing. The Raman data are in agreement with the diffraction results of Fig. 1.

Scanning electron microscopy (SEM) images indicate clear differences in the particle size and the morphology between the undoped and fluorine-added lithium-manganese-oxides, as shown in Fig. 3(a) and (b). The bare particles consist of agglomerated submicron-sized grains with an average particle size of ~5 μm. By contrast, fluorine substitution leads to larger particles of ~10 μm with a smooth surface morphology. These morphological differences affect the contact area with the electrolyte and the Mn-dissolution reaction. Halide salts are known to be effective mineralizing agents, and are often used as a flux in crystal growth [21,33].

The voltage profiles of the undoped and fluorine-substituted cathodes are presented in Fig. 4. The cathodes were tested at 55 °C using coin-type half cells (2016 size) at 0.2 C (=36 mA $g^{-1}$) in the voltage window of 4.5 and 2 V. Both samples display the typical voltage profiles of $o$-$LiMnO_2$-based cathodes. The performances of these samples during 100 cycles are shown in Fig. 5. The undoped $o$-

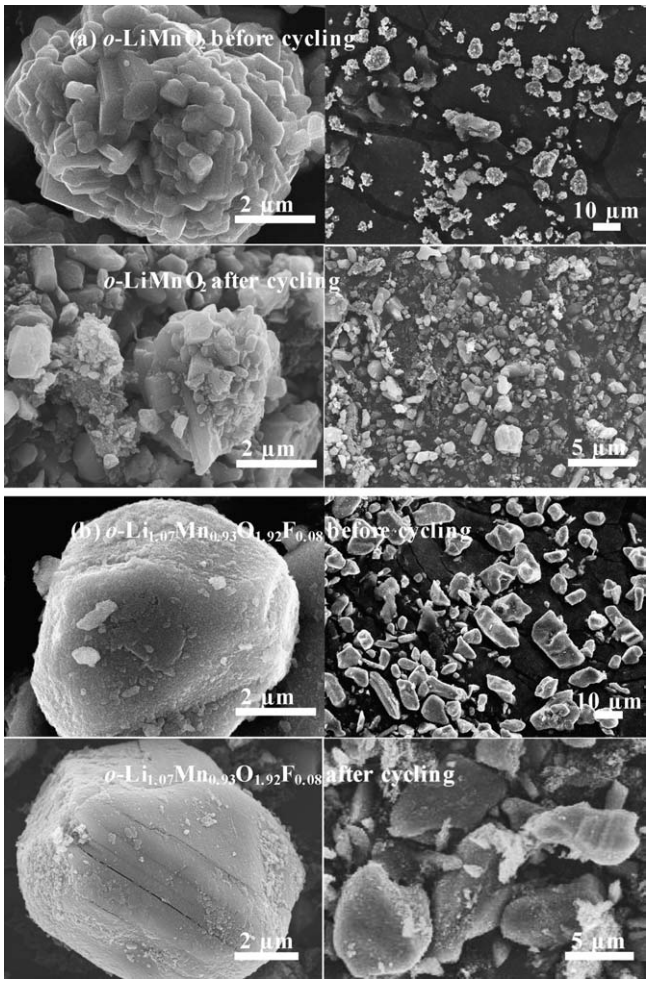


Fig. 3. Scanning electron micrographs of lithium-manganese-oxide powders: (a) bare $o$-$LiMnO_2$; (b) $o$-$Li_{1.07}Mn_{0.93}O_{1.92}F_{0.08}$. Cycled samples are at 2 V discharge state after 100 cycles between 4.5 and 2 V at 55 °C with 0.2 C (=36 mA $g^{-1}$).

$LiMnO_2$ cathode has a maximum capacity of ~203 mAh $g^{-1}$ on the 3rd cycle, and exhibits an average capacity decay of approximately −1.5 mAh $g^{-1}$ per cycle. By contrast, the fluorine-substituted sample, $o$-$Li_{1.07}Mn_{0.93}O_{1.92}F_{0.08}$, has a maximum capacity of ~168 mAh $g^{-1}$ on the 10th cycle, and experiences an average capacity decay of approximately −0.6 mAh $g^{-1}$ per cycle.

The decrease in the maximum capacity by fluorine substitution might be due to the lower theoretical capacity of $o$-$Li_{1.07}Mn_{0.93}O_{1.92}F_{0.08}$ (~257 mAh $g^{-1}$) compared with that of undoped $o$-$LiMnO_2$ (~285 mAh $g^{-1}$). Although the maximum capacity of $o$-$Li_{1.07}Mn_{0.93}O_{1.92}F_{0.08}$ is smaller than that of undoped $o$-$LiMnO_2$, the appropriate fluorine substitution clearly improves the capacity-retention properties. This behaviour agrees well with that reported in the literatures [10,19] with respect to crystallinity and stacking faults.

The rate capability at elevated temperature (55 °C) was tested by varying the discharge rate between 4.5 and 2 V, as shown in Fig. 6(a). The capacity fading is greater at 0.04 C discharge than at 1 C discharge. This can be attributed to the

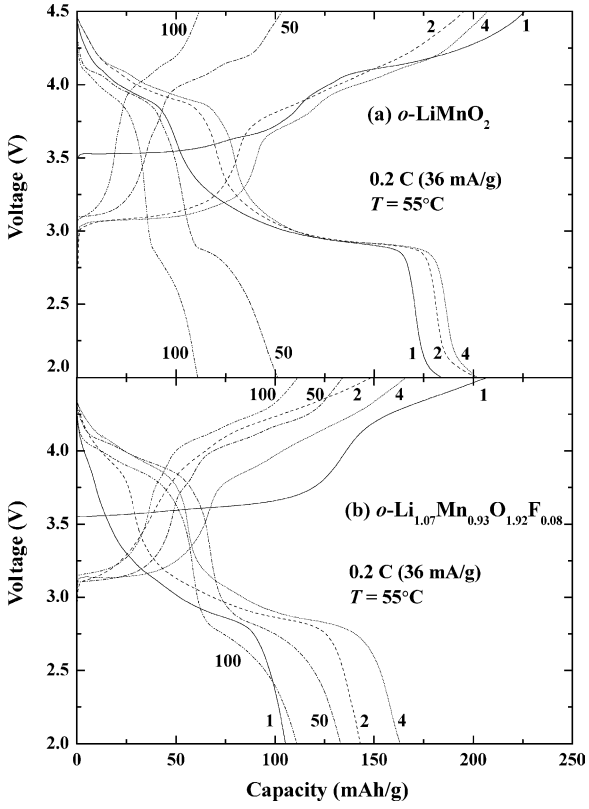


Fig. 4. Voltage profiles of: (a) bare $o$-$LiMnO_2$ cathode and (b) $o$-$Li_{1.07}Mn_{0.93}O_{1.92}F_{0.08}$ cathode between 4.5 and 2 V. C rate is 0.2 C (=36 mA $g^{-1}$).

exposure-time effects of manganese dissolution at a high voltage. Data from cycling at room temperature between 4.5 and 2 V are given in Fig. 6(b). While the average capacity decay for the undoped cathode is approximately −0.6 mAh $g^{-1}$ per cycle, that for $o$-$Li_{1.07}Mn_{0.93}O_{1.92}F_{0.08}$ is negligible (after approximately 40 cycles).

As shown in Fig. 3(a), the particle size of the undoped powders decreases on cycling. On the other hand, the fluorinated powders remain as relatively large particles with a smooth morphology (Fig. 3(b)). A tendency for the particles to crumble during electrochemical cycling will affect the electrical contact and the capacity retention.

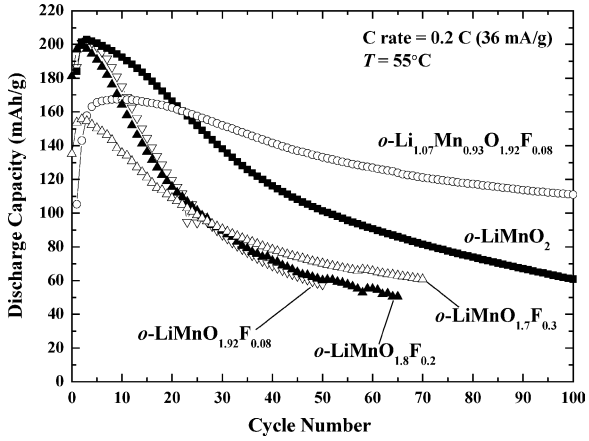


Fig. 5. Cycle-life performances at elevated temperature (55 °C) for orthorhombic lithium-manganese-oxide cathodes with different Li and F doping conditions between 4.5 and 2 V.

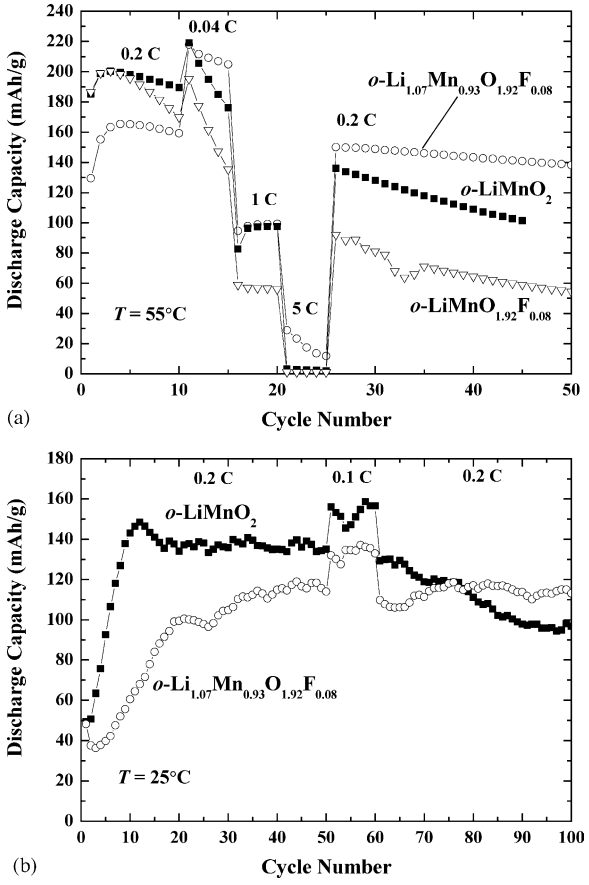


Fig. 6. Plots of: (a) rate-capability tests at elevated temperature (55 °C), and (b) cycle-life performances at room temperature between 4.5 and 2 V.

For the structural characterization of the cycled electrodes, ex situ XRD patterns were obtained (see Fig. 7). After 100 cycles, the cells were kept at a 2 V discharge state at 55 °C.

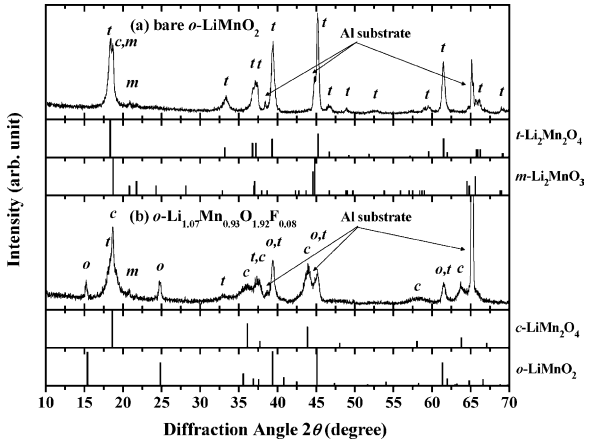


Fig. 7. XRD patterns for undoped $o$-$LiMnO_2$ and $o$-$Li_{1.07}Mn_{0.93}O_{1.92}F_{0.08}$ at 2 V discharge state after 100 cycles between 4.5 and 2 V at 55 °C.

The remarkable difference is that the major phases of the cycled *o*-$Li_{1.07}Mn_{0.93}O_{1.92}F_{0.08}$ are *c*-$LiMn_2O_4$ (cubic) and *o*-$LiMnO_2$, while undoped *o*-$LiMnO_2$ after cycling reports only *t*-$Li_2Mn_2O_4$ (tetragonal). More detailed analyses of the structural properties of cycled electrodes are required.

## 4. Conclusions

Fluorinated lithium-manganese-oxide has been synthesized through a solid-state reaction with Li and F additions. The *o*-$Li_{1.07}Mn_{0.93}O_{1.92}F_{0.08}$ cathode has a well-defined crystallinity with less stacking faults and a larger grain/powder morphology, than undoped *o*-$LiMnO_2$. The fluorine-modified $LiMnO_2$ cathode exhibits improved capacity retention and rate capability at an elevated temperature (55 °C).

## Acknowledgements

The authors thank Jisuk Kim and Mijung Noh at Kumoh National Institute of Technology for their experimental support and Cheil Industries for the supply of the electrolytes. This work was supported by KOSEF through the Research Center for Energy Conversion and Storage at Seoul National University, by the National R&D Program of the Ministry of Science and Technology, and by the Basic Research Program (R01-2004-000-10173-0) of KOSEF.

## References

[1] M.M. Thackeray, W.I.F. David, P.G. Bruce, J.B. Goodenough, Mater. Res. Bull. 18 (1983) 461.
[2] M.M. Thackeray, P.J. Johnson, L.A. de Picciotto, P.G. Bruce, J.B. Goodenough, Mater. Res. Bull. 19 (1984) 179.
[3] J. Cho, M.M. Thackeray, J. Electrochem. Soc. 146 (1999) 3577.
[4] R.J. Gummow, A. de Kock, M.M. Thackeray, Solid State Ionics 69 (1990) 59.
[5] G.G. Amatucci, C.N. Schmutz, A. Blyr, C. Sigala, A.S. Gozdz, D. Larcher, J.M. Tarascon, J. Power Sources 69 (1997) 11.
[6] A. de Kock, M.H. Rossouw, L.A. de Picciotto, M.M. Thackeray, W.I.F. David, S.A. Hull, Mater. Res. Bull. 25 (1990) 657.
[7] J.B. Goodenough, Rev. Chim. Miner. 21 (1981) 435.
[8] J. Cho, Y.J. Kim, T.-J. Kim, B. Park, Chem. Mater. 13 (2001) 18.
[9] J. Cho, Y.J. Kim, T.-J. Kim, B. Park, J. Electrochem. Soc. 149 (2002) A127.
[10] L. Croguennec, P. Deniard, R. Brec, A. Lecerf, J. Mater. Chem. 7 (1997) 511.
[11] Y.-M. Chiang, D.R. Sadoway, Y.-I. Jang, B. Huang, H. Wang, Electrochem. Solid-State Lett. 2 (1999) 107.
[12] J.N. Reimers, E.W. Fuller, E. Rossen, J.R. Dahn, J. Electrochem. Soc. 140 (1993) 3396.
[13] A. Blyr, C. Sigala, G.G. Amatucci, D. Guyomard, Y. Chabre, J.-M. Tarascon, J. Electrochem. Soc. 145 (1998) 194.
[14] D. Aurbach, Y. Gofer, J. Electrochem. Soc. 138 (1991) 3529.
[15] R.J. Gummow, M.M. Thackeray, J. Electrochem. Soc. 141 (1994) 1178.
[16] A.D. Robertson, S.H. Lu, W.F. Howard, J. Electrochem. Soc. 144 (1997) 3505.
[17] L. Croguennec, P. Deniard, R. Brec, J. Electrochem. Soc. 144 (1997) 3323.
[18] L. Croguennec, P. Deniard, R. Brec, A. Lecerf, J. Mater. Chem. 5 (1995) 1919.
[19] J.-M. Kim, H.-T. Chung, J. Power Sources 115 (2003) 125.
[20] Y.-I. Jang, B. Huang, H. Wang, D.R. Sadoway, Y.-M. Chiang, J. Electrochem. Soc. 146 (1999) 3217.
[21] P.S. Whitfield, I.J. Davidson, J. Electrochem. Soc. 147 (2000) 4476.
[22] W. Xiaomei, Z. Xiangfu, Y. Qinghe, J. Zhongkao, W. Haoqing, J. Fluorine Chem. 107 (2001) 39.
[23] K. Kubo, M. Fujiwara, S. Yamada, S. Arai, M. Kanda, J. Power Sources 68 (1997) 553.
[24] K. Kubo, S. Arai, S. Yamada, M. Kanda, J. Power Sources 81 (1999) 599.
[25] Y. Xia, Y. Hideshima, N. Kumada, M. Nagano, M. Yoshio, J. Power Sources 24 (1998) 24.
[26] G.G. Amatucci, N. Pereira, T. Zheng, J.-M. Tarascon, J. Electrochem. Soc. 148 (2001) A171.
[27] A.R. Naghash, J.Y. Lee, Electrochim. Acta 46 (2001) 941.
[28] F. Roulland, R. Terras, G. Allainmat, M. Pollet, S. Marinel, J. Eur. Ceram. Soc. 24 (2004) 1019.
[29] S. Marinel, M. Pollet, G. Desgardin, J. Mater. Sci.: Mater. Electron. 13 (2002) 149.
[30] S. Jouanneau, J.R. Dahn, J. Electrochem. Soc. 151 (2004) A1749.
[31] C.M. Julien, Ionics 6 (2000) 30.
[32] C.M. Julien, M. Massot, Mater. Sci. Eng. B 100 (2003) 69.
[33] P.J. Hirst, A. Drake, M. Rand, J.S. Abell, Physica C 235–240 (1994) 371.